ROYAL SOCIETY
OF CHEMISTRY

PAPER

Check for updates

Engineering a "nanonet"-reinforced polymer electrolyte for long-life Li–O₂ batteries†

Changtai Zhao, [ID] [a] Jianneng Liang,[a] Yang Zhao,[a] Jing Luo,[a] Qian Sun,[a] Yulong Liu,[a] Xiaoting Lin,[a] Xiaofei Yang,[a] Huan Huang,[c] Li Zhang,[b] Shangqian Zhao,[b] Shigang Lu[b] and Xueliang Sun [ID] *[a]

Safe, high-energy-density and long-life Li metal batteries (LMBs) are highly attractive as a power source. However, the development of LMBs encounters serious challenges due to the formation of Li dendrites and the leakage and flammability of organic liquid electrolytes. Herein, a novel nanowire-film-reinforced hybrid gel polymer electrolyte (HGPE) is developed. The interconnected porous nanowire film as the backbone not only strengthens the mechanical structure of GPEs but also ensures the continuity for Li⁺ conduction. The designed HGPE can simultaneously achieve the suppression of Li dendrites and high ionic conductivity (1.04×10^{-3} S cm^{-1}). The films with controllable thicknesses offer the ability to prepare ultrathin HGPEs with great mechanical properties. With these merits, the Li metal symmetric cells exhibit significantly enhanced cycling stability for over 2100 h with low overpotential. The Li–O₂ battery using the HGPE also delivers an ultralong cycle life of up to 494 cycles. The present study may open a new window for reinforcing GPEs and offer an opportunity for developing quasi-solid-state LMBs.

Introduction

Lithium (Li)-ion batteries (LIBs) have been the dominant power source in electronics and electric vehicles since their commercialization, prompting the development of modern electrical applications.[1–4] Nevertheless, LIBs are now encountering a bottleneck related to energy density due to the limited specific capacities of anode and cathode materials. The currently available battery designs cannot fulfill the ever-growing demand for higher energy density. Thus, there is an urgent call for innovative battery chemistries beyond the state-of-the-art LIBs.[5,6] Li metal batteries (LMBs), owing to the high theoretical capacity (3860 mA h g⁻¹) and the lowest electrochemical potential (−3.04 V *vs.* the standard hydrogen electrode) of Li metal, have been resurrected and have attracted intensive research interest.[7–9] Among all LMB systems with different cathode options, Li–O₂ batteries feature the highest theoretical energy density of up to 3500 W h kg⁻¹ and show great promise to meet the needs of high energy density.[10–12]

Conventional organic liquid electrolytes (LEs) have caused serious safety concerns for Li–O₂ batteries,[13–17] and the replacement of organic LEs by (quasi) solid-state electrolytes (SSEs) can be an effective strategy to address the

challenges.[15,18–23] Hazards such as Li dendrite formation, possible leakage problem, and flammability of organic LEs are especially exacerbated in an open system like Li–O₂ batteries.[21,24–27] Among the alternative candidates to LEs, gel polymer electrolytes (GPEs) have drawn considerable attention due to their comparable ionic conductivity, low cost, and excellent processability. GPEs can function as both an electrolyte and separator.[28–31] Evident advantages including low interfacial resistance, regulated Li deposition behavior, mitigation of O₂ crossover, and alleviation of electrolyte evaporation are beneficial for the development of advanced Li–O₂ batteries.

However, the large thickness of GPE films can significantly undermine the energy density of batteries. Not only is the fabrication of ultrathin GPEs challenging, but also are the mechanical strengths of ultrathin GPEs generally too weak to suppress Li dendrites.[32,33] Even though addition of inorganic fillers into GPEs is one approach to overcome the limitations, powder fillers tend to agglomerate and distribute unevenly in the GPE.[13,34–39] Drawbacks are insufficient mechanical reinforcement, reduced efficacy for Li dendrite suppression, and insufficient ionic conductivity.[40–42] To simultaneously achieve good mechanical strength and high ionic conductivity, the introduction of a coherent skeleton with free-standing, porous, and lightweight properties, for instance a nanowire film, is a promising strategy.[32,41]

Herein, an interconnected nanowire-film-reinforced hybrid GPE (HGPE) was developed as the electrolyte and separator for Li–O₂ batteries. The free-standing MnOOH@Al₂O₃ skeleton is lightweight, coherent, and highly porous. The tunable thickness

ᵃDepartment of Mechanical and Materials Engineering, University of Western Ontario, London, ON, N6A 5B9, Canada. E-mail: xsun9@uwo.ca

ᵇChina Automotive Battery Research Institute, Beijing, 100088, P. R. China

ᶜGlabat Solid-State Battery Inc., London, ON, N6G 4X8, Canada

This journal is © The Royal Society of Chemistry 2019

J. Mater. Chem. A, 2019, 7, 24947–24952 | 24947

and favorable mechanical properties of the skeleton have enabled the fabrication of an ultrathin HGPE and the suppression of Li dendrites. The high porosity of the skeleton also ensures a high proportion and coherence of the GPE content within the HGPE, leading to a high ionic conductivity of 1.04×10^{-3} S cm^{-1} at room temperature. Owing to these merits, the Li metal symmetric cells with the HGPE exhibited a significantly enhanced cycling stability of up to 2100 h with low overpotential. The Li–O$_2$ battery also delivered an ultralong cycle life of 494 cycles.

Experimental

Synthesis of the MnOOH@Al$_2$O$_3$ film

MnOOH nanowires were synthesized by a hydrothermal method.[43] Typically, 21 mg of polyvinylpyrrolidone (PVP, M_w: 55 000) and 42 mg of KMnO$_4$ were dissolved in 40 mL of deionized water under continuous stirring for 0.5 h. Then, the solution was transferred into a 50 mL Teflon-lined stainless-steel autoclave and kept at 140 °C for 25 h. MnOOH nanowires were obtained by centrifugation separation and drying processes. The MnOOH nanowire film was fabricated by vacuum filtration of the solution with MnOOH nanowires. The thickness of the film can be regulated by controlling the amounts of MnOOH nanowires in the solution. Then, the hybrid film of MnOOH@Al$_2$O$_3$ was prepared by atomic layer deposition according to our previous reports.[44]

Synthesis of the HGPE

The HGPE was prepared by a solution casting method. Typically, poly(vinylidene fluoride-co-hexafluoropropylene) (PVDF-HFP) polymer (M_w: 400 000) was dissolved in acetone by vigorous stirring. Then, tetraethylene glycol dimethyl ether (TEGDME), LiClO$_4$, and LiNO$_3$ were added into the solution and continuously stirred overnight. The resulting solution was cast onto a film of MnOOH@Al$_2$O$_3$ on a polytetrafluoroethylene substrate and dried at room temperature for three days to remove acetone solvent. For comparison, pure GPE was also fabricated in the absence of the film under the same conditions. The air electrode of Ni foam@Co$_3$O$_4$–RuO$_2$ was prepared according to our previous report.[45]

Materials characterization

The thickness, structure, and composition of the HGPE were characterized by scanning electron microscopy (SEM) (Hitachi S-4800), transmission electron microscopy (TEM) (Tecnai G220), and X-ray diffraction (XRD) (D/Max-III-type, Cu Kα X-ray source).

Electrochemical measurements

Ni foam@Co$_3$O$_4$–RuO$_2$ was free-standing and used as the cathode directly. The areal loading of the RuO$_2$ catalyst is about 0.28 mg cm^{-2}. The as-prepared HGPE serves as both the electrolyte and separator in quasi-solid-state cells. The electrochemical performances of Li–O$_2$ batteries were evaluated by assembling Swagelok-type cells and tested on an Arbin battery testing system in 1 atm O$_2$. The electrochemical impedance spectroscopy (EIS) tests were performed on a Bio-Logic electrochemical workstation at open circuit potential.

Results and discussion

The synthesis process of the HGPE is schematically shown in Scheme 1a. Ultralong MnOOH nanowires were synthesized by a hydrothermal method. The MnOOH nanowires were assembled into a free-standing film by vacuum filtration.[43] The film thickness is tunable to as thin as 23 μm, which allows the flexibility in fabrication and designs for HGPEs with controlled thickness. A protective layer of Al$_2$O$_3$ was deposited on the surface of MnOOH nanowires by atomic layer deposition to prevent the reaction between MnOOH and Li metal and ensure electrical insulation of the skeleton. The fabrication of the HGPE film was finished by solution casting the GPE. A solution of PVDF-HFP, TEGDME, LiClO$_4$ salt and the LiNO$_3$ additive in acetone was infused into the MnOOH@Al$_2$O$_3$ skeleton, followed by drying at room temperature for three days. As shown in Scheme 1b, the pure GPE is translucent, and the obtained HGPE adopts the brown color of the skeleton. The as-prepared HGPE is free-standing and flexible, which can be directly used as both the electrolyte and separator in Li–O$_2$ batteries. The MnOOH@Al$_2$O$_3$ skeleton is expected to mechanically suppress Li dendrite growth in the HGPE, as an advantage over the GPE (Scheme 1c).

As shown in Fig. 1a and S1,† the MnOOH nanowires were more than 10 μm in length and 50–100 nm in diameter. The long and slender MnOOH nanowires were interconnected to construct a strong skeleton network that featured a free-standing and flexible structure (Fig. 1b). High-magnification SEM images reveal the porosity of the film at the micro-scale (Fig. 1c). The porosity was determined to be 91.1% based on the density of 4.32×10^6 g m^{-3} of γ-MnOOH, indicating that a large amount of GPE can be filled. The skeleton still maintained the original structure after Al$_2$O$_3$ coating (Fig. 1e and f). The uniform coating of Al$_2$O$_3$ was confirmed by energy-dispersive X-ray spectroscopy (EDX) elemental mappings of the MnOOH@Al$_2$O$_3$ film (Fig. S2†). The Al$_2$O$_3$ layer on the surface of MnOOH nanowires serves as a protective layer for preventing the reaction between Li metal and MnOOH and ensuring the electrical insulation of the hybrid film. The MnOOH@Al$_2$O$_3$ framework helped to reinforce the mechanical properties of the
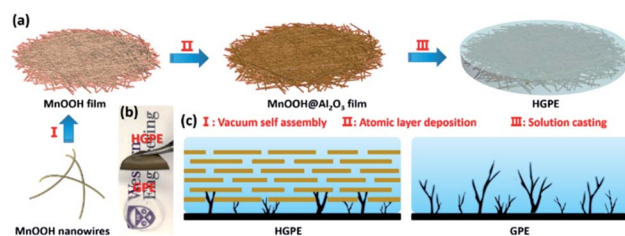
Scheme 1 (a) Schematic illustration of the synthesis process of the HGPE. (b) Digital photo of the as-prepared GPE and HGPE. (c) Schematic comparison of the Li dendrite growth in the HGPE and GPE.
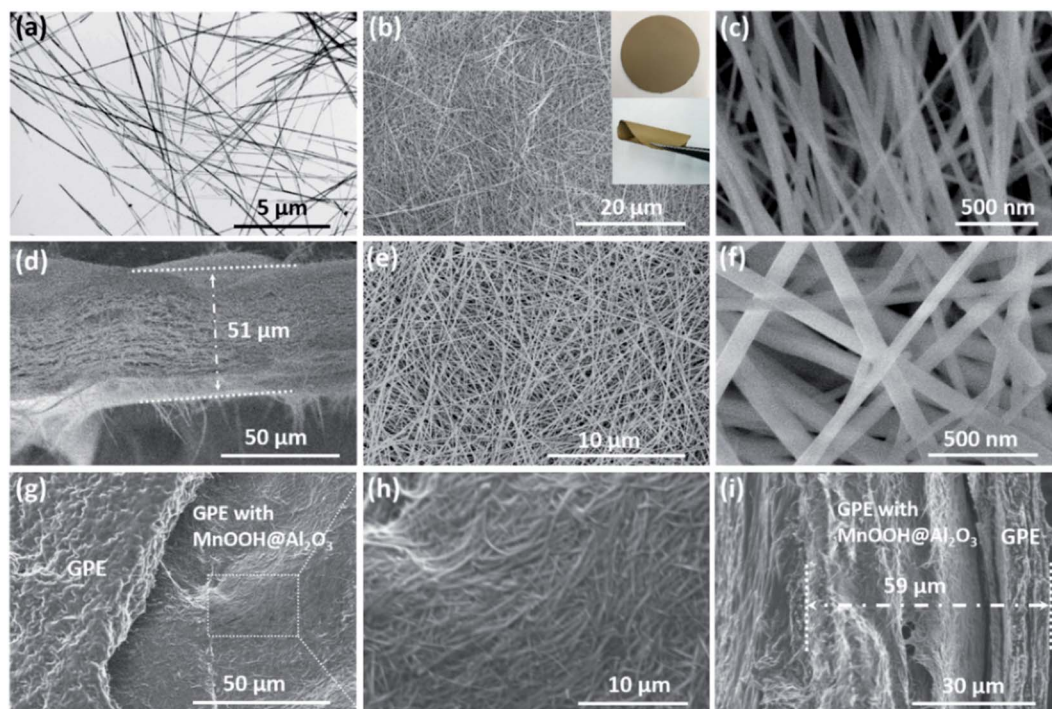
24948 | J. Mater. Chem. A, 2019, 7, 24947–24952

This journal is © The Royal Society of Chemistry 2019

Fig. 1 Morphology and structure of the as-prepared skeleton and HGPE. (a) TEM and (b–d) SEM images of the MnOOH skeleton. The insets in (b) show the digital photographs of the MnOOH film. (e and f) SEM images of the MnOOH@Al$_2$O$_3$ film. (g and h) Top-view and (i) cross-section SEM images of the HGPE.

HGPE and suppress Li dendrites. The interconnected void space allowed the continuity of the GPE that ensured high ionic conductivity. Moreover, the film can be made with different thicknesses ranging from 23 μm to above (Fig. S3† and 1d). Correspondingly, the HGPE can be cast with different thicknesses while maintaining strong mechanical strength and flexibility. The areal mass of the MnOOH@Al$_2$O$_3$ film with a thickness of 51 μm is about 1.1 mg cm^{-2}, featuring low volume density. In spite of the low density and thin thickness, the film features a great tensile strength. As shown in Fig. S4,† it can bear a weight of 57 g, which is 2700 times its weight, indicting the great mechanical strength.

As shown in Fig. 1g–i and Scheme 1c, the as-prepared HGPE features a sandwich-type structure with two thin outer layers of the pure GPE and an interior layer of the GPE impregnated MnOOH@Al$_2$O$_3$. The presence of the pure GPE on the outside enables the good wettability with electrodes and thus low interfacial resistance.[46] The interior film skeleton is responsible for suppressing Li dendrites as described in Scheme 1c.[40] And the complete filling of the GPE in the skeleton guaranteed a comparably high ionic conductivity for the HGPE (1.04×10^{-3} S cm^{-1}) as to the pure GPE (3.48×10^{-3} S cm^{-1}).[35,40,41] The XRD pattern of the HGPE shows the characteristic peaks from the GPE and MnOOH, confirming the coexistence of all components (Fig. S6†). The weak intensity of the MnOOH peaks compared to the GPE characteristics was also an indication of the dominant coverage of the GPE on the surface. Depending on the thickness of the MnOOH@Al$_2$O$_3$ skeleton, the HGPE is tunable (Fig. 1i and S7†).

In order to evaluate the applicability of the HGPE, electrochemical properties were investigated. Here, the HGPE with a film of a thickness of 51 μm was selected for investigations compared to the pure GPE. The interfacial resistance against the Li metal anode was examined by impedance analysis of Li metal symmetric cells. As shown in Fig. 2a, the HPGE exhibited a low interfacial resistance of 161 Ω against the Li metal anode, which was in the same order of magnitude as the 117 Ω of the pure GPE. When cycling the symmetric cells, the slightly higher interfacial resistance and lower ionic conductivity of the HPGE than the pure GPE initially caused an increase in overpotential, but the stable cycle life was substantially longer. Fig. 2b–d show the cycling results at a current density of 0.1 mA cm^{-2} with a limited capacity of 0.3 mA h cm^{-2}. The cell with the pure GPE encountered a short circuit after 280 h of cycling, while the cell with the HGPE showed a significantly extended cycle life of up to 2100 h. The enhanced cycling stability highlighted the effect of the MnOOH@Al$_2$O$_3$ skeleton as ramparts for suppressing Li dendrite growth. The effect was more obvious with a larger cycling capacity of 0.5 mA h cm^{-2} at a higher current density of 0.2 mA cm^{-2}. As shown in Fig. 2e, the cell with the HGPE cycled stably for more than 450 h, in contrast to the rapid short circuit of the cell with the pure GPE within 70 h. As shown in Fig. S8,† with the increase of current density, the cell with the HGPE shows increased overpotential, but maintains a stable shape. When the current density is returned to 0.1 mA cm^{-2} again, the voltage curve also recovers to the original level. By contrast, the cell with the pure GPE shows unstable voltage curves at increased current densities, accompanied by short circuits. This
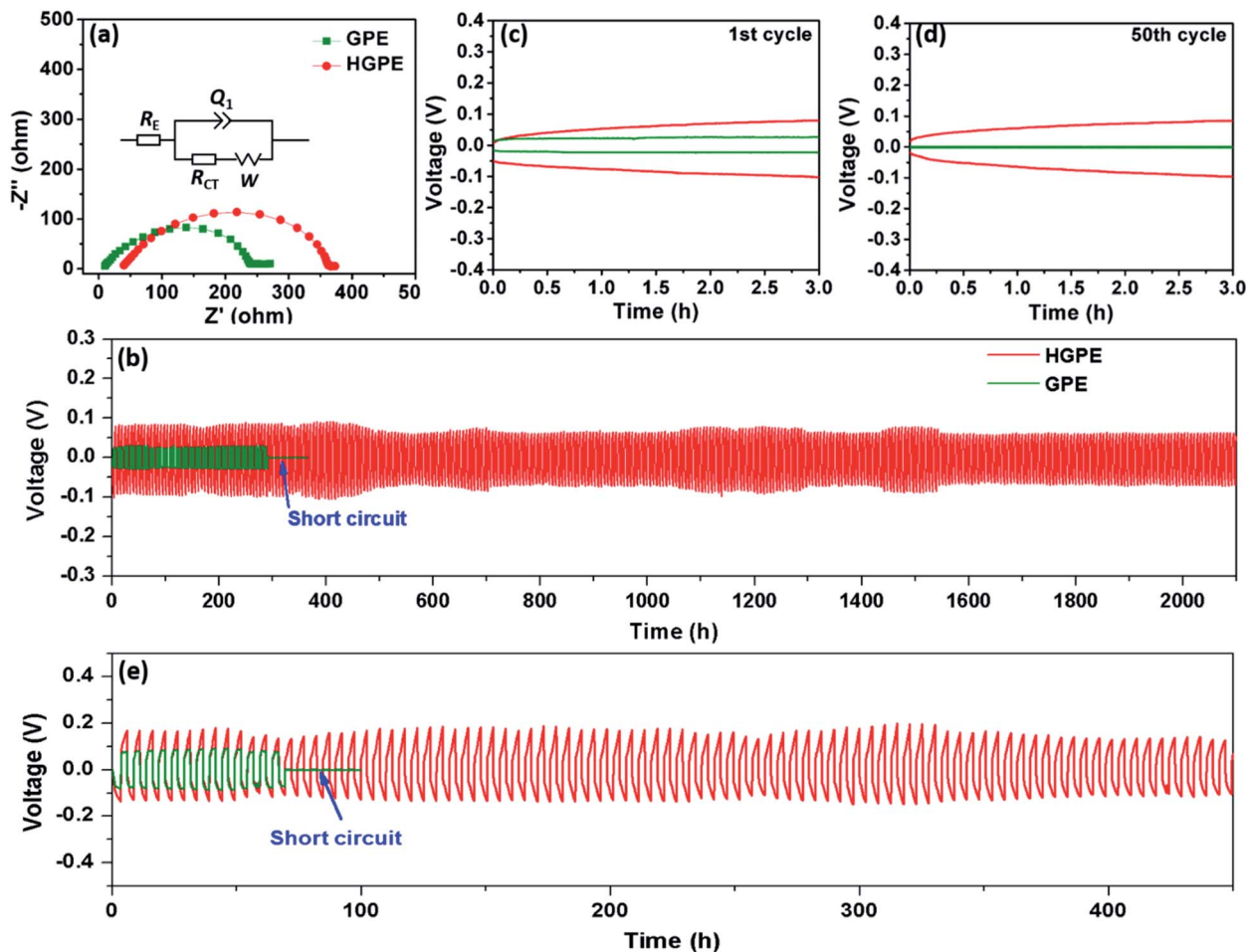
Fig. 2 Electrochemical performance of Li metal symmetric cells with the HGPE and GPE. (a) Nyquist plots of the Li metal symmetric cells with the HGPE and GPE. (b) The cycling stability of Li metal symmetric cells with the HGPE and GPE at a current density of 0.1 mA cm^{-2} with a limited capacity of 0.3 mA h cm^{-2}. The corresponding discharge/charge profiles in the (c) 1st cycle and (d) 50th cycle. (e) The cycling stability of Li metal symmetric cells with the HGPE and GPE at a current density of 0.2 mA cm^{-2} with a limited capacity of 0.5 mA h cm^{-2}.

demonstrates the effect of the support for enhancing the cycle performance, especially at a large current density. The stable cycling performance of the skeleton reinforced HGPE against Li metal shows a promising first step for developing long-life quasi-solid-state Li–O$_2$ batteries.

In order to further evaluate the electrochemical performance of the proposed HGPE in Li–O$_2$ batteries, a high-efficiency air electrode was required. Here, the air electrode possessed a hierarchical microstructure with RuO$_2$ nanoparticles on the top of Co$_3$O$_4$ nanowires that were grown on a Ni foam substrate (Ni foam@Co$_3$O$_4$–RuO$_2$). The morphology and structure of the as-prepared air electrode are shown in Fig. S9.† The composite air electrode featured interconnected pores, and the RuO$_2$ nanoparticles with a diameter of *ca.* 3 nm were uniformly anchored on the surface of Co$_3$O$_4$ nanowires. By minimizing the limitations in the air electrode, the role and advantages of the HGPE in Li–O$_2$ batteries can be better clarified.

The electrochemical performance of Li–O$_2$ batteries with the designed HGPE and Ni foam@Co$_3$O$_4$–RuO$_2$ air electrode was evaluated by EIS and galvanostatic discharge/charge tests. As

shown in Fig. S11a,† the Nyquist plot indicated a low initial charge transfer resistance of the Li–O$_2$ battery, indicating great compatibility with the air electrode.[47] As shown in Fig. S11b,† the Li–O$_2$ battery delivered a high areal capacity of 3.2 mA h cm^{-2} at a current density of 0.1 mA cm^{-2}. Meanwhile, the
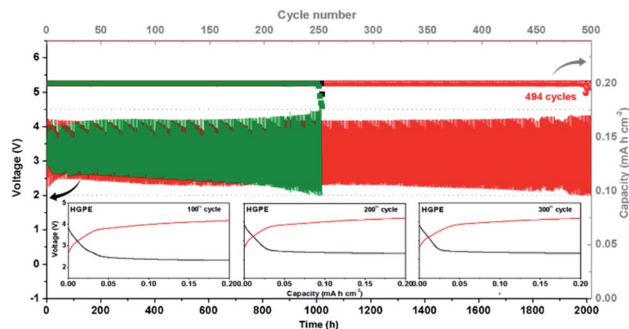

Fig. 3 Electrochemical performance of Li–O$_2$ batteries with the HGPE and GPE at a current density of 0.1 mA cm^{-2} with a limited capacity of 0.2 mA h cm^{-2}.
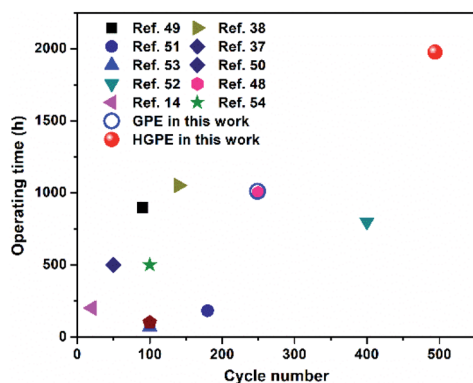
Fig. 4 The comparison of the operating time and cycle number of Li–O$_2$ batteries in the present work and previous studies in the literature.

cycling performance was tested at a current density of 0.1 mA cm^{-2} with a limited capacity of 0.2 mA h cm^{-2}, and the results are shown in Fig. 3. Notably, the Li–O$_2$ battery exhibited an ultralong cycling life of up to 494 cycles without capacity decay and a stable operation time of nearly 2000 h, which are longer than the 249 cycles and 1010 h of the battery with the pure GPE. The discharge/charge profiles show a low charge overpotential, highlighting the high catalytic activity of RuO$_2$ nanoparticles and the high stability of the system.[43] The discharge/charge profiles show decreasing overpotential with the increase of cycle number, which may be attributed to the further improved compatibility. For better evaluating the electrochemical performance of the Li–O$_2$ battery with the HGPE and the high-efficiency air electrode, the cycling performance of the present work and the reported results from the literature are compared in Fig. 4. The Li–O$_2$ battery performance of this study shows the longest operating time and the highest cycle number, further highlighting the advance of this HGPE and high-efficiency air electrode.[13,37,38,48–54]

Conclusions

In summary, we have successfully developed a novel class of nanowire-film-reinforced hybrid gel polymer electrolytes for application in Li–O$_2$ batteries. To address the drawback of weak mechanical strength of GPEs, a MnOOH@Al$_2$O$_3$ skeleton was designed to uniformly strengthen the mechanical properties of HGPEs, avoiding the inhomogeneity of powder fillers. The controllable thickness of the MnOOH@Al$_2$O$_3$ films enables the fabrication of an ultrathin HGPE with great mechanical properties. The highly porous network also has ensured the continuity of the filled GPE for high ionic conductivity. In this context, the suppression of Li dendrites and high ionic conductivity are simultaneously achieved in the HGPE. Benefiting from these merits, the Li metal symmetric cells with the HGPE exhibited stable cyclability for over 2100 h. The Li–O$_2$ battery also delivered an ultralong cycle life of up to 494 cycles. The outstanding electrochemical performance also indicated the capability of the HGPE to effectively suppress Li dendrite growth. Here, the MnOOH nanowire was chosen as an example

to show the fact that the assembled porous film with a free-standing structure can be used as the skeleton to simultaneously achieve suppression of Li dendrites and high ionic conductivity of the GPE. Actually, an ionically conductive nanowire-film, for example LLZO nanowires, may be a better candidate for preparing HGPEs. The present study may open a new way for reinforcing GPEs and offer an opportunity for developing quasi-solid-state LMBs.

Author contributions

C. Zhao and X. Sun conceived the project and designed the experiments. C. Zhao, J. Liang, and Y. Zhao carried out the synthesis of materials and the test of electrochemical performance. Q. Sun, Y. Liu, X. Lin, X. Yang, H. Huang, L. Zhang, S. Zhao, and S. Lu participated in data analysis and discussion. C. Zhao and X. Sun co-wrote the paper. J. Luo polished the manuscript; X. Sun supervised the overall project. All authors discussed the results and commented on the manuscript.

Conflicts of interest

There are no conflicts to declare.

Acknowledgements

Notes and references

1 C. Zhao, C. Yu, M. Zhang, Q. Sun, S. Li, M. Norouzi Banis, X. Han, Q. Dong, J. Yang, G. Wang, X. Sun and J. Qiu, *Nano Energy*, 2017, **41**, 66–74.

2 J. Lu, L. Li, J.-B. Park, Y.-K. Sun, F. Wu and K. Amine, *Chem. Rev.*, 2014, **114**, 5611–5640.

3 C. Zhao, C. Yu, B. Qiu, S. Zhou, M. Zhang, H. Huang, B. Wang, J. Zhao, X. Sun and J. Qiu, *Adv. Mater.*, 2018, **30**, 1702486.

4 C. Zhao, C. Yu, M. Zhang, H. Huang, S. Li, X. Han, Z. Liu, J. Yang, W. Xiao, J. Liang, X. Sun and J. Qiu, *Adv. Energy Mater.*, 2017, **7**, 1602880.

5 P. G. Bruce, S. A. Freunberger, L. J. Hardwick and J.-M. Tarascon, *Nat. Mater.*, 2011, **11**, 19.

6 X.-B. Cheng, R. Zhang, C.-Z. Zhao and Q. Zhang, *Chem. Rev.*, 2017, **117**, 10403–10473.

7 C. Zhao, C. Yu, S. Li, W. Guo, Y. Zhao, Q. Dong, X. Lin, Z. Song, X. Tan, C. Wang, M. Zheng, X. Sun and J. Qiu, *Small*, 2018, **14**, 1803310.

8 D. Lin, Y. Liu and Y. Cui, *Nat. Nanotechnol.*, 2017, **12**, 194.

9 C. Zhao, C. Yu, M. Zhang, J. Yang, S. Liu, M. Li, X. Han, Y. Dong and J. Qiu, *J. Mater. Chem. A*, 2015, **3**, 21842–21848.

10 C. Yu, C. Zhao, S. Liu, X. Fan, J. Yang, M. Zhang and J. Qiu, *Chem. Commun.*, 2015, **51**, 13233–13236.

11 C. Zhao, C. Yu, S. Li, J. Yang, X. Fan, H. Huang and J. Qiu, *Adv. Funct. Mater.*, 2015, **25**, 6913–6920.

12 P. Lou, C. Li, Z. Cui and X. Guo, *J. Mater. Chem. A*, 2016, **4**, 241–249.

13 G. A. Elia and J. Hassoun, *Sci. Rep.*, 2015, **5**, 12307.

14 X.-P. Zhang, Z.-Y. Wen and T. Zhang, *J. Mater. Chem. A*, 2018, **6**, 12945–12949.

15 J. Yi, S. Guo, P. He and H. Zhou, *Energy Environ. Sci.*, 2017, **10**, 860–884.

16 H. Kitaura and H. Zhou, *Energy Environ. Sci.*, 2012, **5**, 9077–9084.

17 L. Yang, W. Xiaogang, D. Shanmu, C. Xiao and C. Guanglei, *Adv. Energy Mater.*, 2016, **6**, 1600751.

18 N. Bonnet-Mercier, R. A. Wong, M. L. Thomas, A. Dutta, K. Yamanaka, C. Yogi, T. Ohta and H. R. Byon, *Sci. Rep.*, 2014, **4**, 7127.

19 T. Zhang and H. Zhou, *Nat. Commun.*, 2013, **4**, 1817.

20 X. B. Zhu, T. S. Zhao, Z. H. Wei, P. Tan and L. An, *Energy Environ. Sci.*, 2015, **8**, 3745–3754.

21 Y. Liu, P. He and H. Zhou, *Adv. Energy Mater.*, 2018, **8**, 1701602.

22 X. Wang, D. Zhu, M. Song, S. Cai, L. Zhang and Y. Chen, *ACS Appl. Mater. Interfaces*, 2014, **6**, 11204–11210.

23 H. Wu, J. Wang, Y. Zhao, X. Zhang, L. Xu, H. Liu, Y. Cui, Y. Cui and C. Li, *Sustainable Energy Fuels*, 2019, **3**, 2642–2656.

24 X. Zhu, T. Zhao, P. Tan, Z. Wei and M. Wu, *Nano Energy*, 2016, **26**, 565–576.

25 X. B. Zhu, T. S. Zhao, Z. H. Wei, P. Tan and G. Zhao, *Energy Environ. Sci.*, 2015, **8**, 2782–2790.

26 Y. Wang and H. Zhou, *Energy Environ. Sci.*, 2011, **4**, 1704–1707.

27 M. Balaish, E. Peled, D. Golodnitsky and Y. Ein-Eli, *Angew. Chem., Int. Ed.*, 2015, **54**, 436–440.

28 T. Liu, Z. Chang, Y. Yin, K. Chen, Y. Zhang and X. Zhang, *Solid State Ionics*, 2018, **318**, 88–94.

29 J. Zhang, B. Sun, X. Xie, K. Kretschmer and G. Wang, *Electrochim. Acta*, 2015, **183**, 56–62.

30 C. V. Amanchukwu, H.-H. Chang, M. Gauthier, S. Feng, T. P. Batcho and P. T. Hammond, *Chem. Mater.*, 2016, **28**, 7167–7177.

31 X. Y. Yang, J. J. Xu, Z. W. Chang, D. Bao, Y. B. Yin, T. Liu, J. M. Yan, D. P. Liu, Y. Zhang and X. B. Zhang, *Adv. Energy Mater.*, 2018, **8**, 1702242.

32 L. Leng, X. Zeng, P. Chen, T. Shu, H. Song, Z. Fu, H. Wang and S. Liao, *Electrochim. Acta*, 2015, **176**, 1108–1115.

33 X. Cheng, J. Pan, Y. Zhao, M. Liao and H. Peng, *Adv. Energy Mater.*, 2018, **8**, 1702184.

34 C.-Z. Zhao, X.-Q. Zhang, X.-B. Cheng, R. Zhang, R. Xu, P.-Y. Chen, H.-J. Peng, J.-Q. Huang and Q. Zhang, *Proc. Natl. Acad. Sci. U. S. A.*, 2017, **114**, 11069–11074.

35 J. Bae, Y. Li, J. Zhang, X. Zhou, F. Zhao, Y. Shi, J. B. Goodenough and G. Yu, *Angew. Chem., Int. Ed.*, 2018, **57**, 2096–2100.

36 Z. Tu, Y. Kambe, Y. Lu and L. A. Archer, *Adv. Energy Mater.*, 2014, **4**, 1300654.

37 J. Yi, S. Wu, S. Bai, Y. Liu, N. Li and H. Zhou, *J. Mater. Chem. A*, 2016, **4**, 2403–2407.

38 W.-B. Luo, S.-L. Chou, J.-Z. Wang, Y.-M. Kang, Y.-C. Zhai and H.-K. Liu, *Chem. Commun.*, 2015, **51**, 8269–8272.

39 S. Wu, J. Yi, K. Zhu, S. Bai, Y. Liu, Y. Qiao, M. Ishida and H. Zhou, *Adv. Energy Mater.*, 2017, **7**, 1601759.

40 P. Yao, B. Zhu, H. Zhai, X. Liao, Y. Zhu, W. Xu, Q. Cheng, C. Jayyosi, Z. Li, J. Zhu, K. M. Myers, X. Chen and Y. Yang, *Nano Lett.*, 2018, **18**, 6113–6120.

41 D. Lin, P. Y. Yuen, Y. Liu, W. Liu, N. Liu, R. H. Dauskardt and Y. Cui, *Adv. Mater.*, 2018, **30**, 1802661.

42 J. Hu, J. Tian and C. Li, *ACS Appl. Mater. Interfaces*, 2017, **9**, 11615–11625.

43 C. Zhao, C. Yu, M. N. Banis, Q. Sun, M. Zhang, X. Li, Y. Liu, Y. Zhao, H. Huang, S. Li, X. Han, B. Xiao, Z. Song, R. Li, J. Qiu and X. Sun, *Nano Energy*, 2017, **34**, 399–407.

44 Y. Zhao, L. V. Goncharova, A. Lushington, Q. Sun, H. Yadegari, B. Wang, W. Xiao, R. Li and X. Sun, *Adv. Mater.*, 2017, **29**, 1606663.

45 C. Zhao, J. Liang, Q. Sun, J. Luo, Y. Liu, X. Lin, Y. Zhao, H. Yadegari, M. N. Banis, R. Li, H. Huang, L. Zhang, R. Yang, S. Lu and X. Sun, *Small Methods*, 2019, **3**, 1800437.

46 B. Kumar, J. Kumar, R. Leese, J. P. Fellner, S. J. Rodrigues and K. M. Abraham, *J. Electrochem. Soc.*, 2010, **157**, A50–A54.

47 H. Kitaura and H. Zhou, *Sci. Rep.*, 2015, **5**, 13271.

48 X. Zou, Q. Lu, Y. Zhong, K. Liao, W. Zhou and Z. Shao, *Small*, 2018, **14**, 1801798.

49 T. Liu, Q.-C. Liu, J.-J. Xu and X.-B. Zhang, *Small*, 2016, **12**, 3101–3105.

50 C. Wu, C. Liao, T. Li, Y. Shi, J. Luo, L. Li and J. Yang, *J. Mater. Chem. A*, 2016, **4**, 15189–15196.

51 L. Wang, Y. Zhang, J. Pan and H. Peng, *J. Mater. Chem. A*, 2016, **4**, 13419–13424.

52 Z. Guo, C. Li, J. Liu, Y. Wang and Y. Xia, *Angew. Chem., Int. Ed.*, 2017, **56**, 7505–7509.

53 Y. Zhang, L. Wang, Z. Guo, Y. Xu, Y. Wang and H. Peng, *Angew. Chem., Int. Ed.*, 2016, **55**, 4487–4491.

54 Q.-C. Liu, T. Liu, D.-P. Liu, Z.-J. Li, X.-B. Zhang and Y. Zhang, *Adv. Mater.*, 2016, **28**, 8413–8418.

24952 | *J. Mater. Chem. A*, 2019, **7**, 24947–24952

This journal is © The Royal Society of Chemistry 2019